Journal of Power Sources 242 (2013) 790–796

Contents lists available at SciVerse ScienceDirect

Journal of Power Sources

journal homepage: www.elsevier.com/locate/jpowsour

Influence of $(La,Sr)MnO_{3+\delta}$ cathode composition on cathode/electrolyte interfacial structure during long-term operation of solid oxide fuel cells

Toshiaki Matsui*, Yuichi Mikami, Hiroki Muroyama, Koichi Eguchi

Department of Energy and Hydrocarbon Chemistry, Graduate School of Engineering, Kyoto University, Nishikyo-ku, Kyoto 615-8510, Japan

HIGHLIGHTS

- Impact of LSM composition on structural change during prolonged operation was studied.
- The densification of cathode layer was observed for A-site deficient LSMs.
- The $P(O_2)$ gradient at the interface under polarization is the major driving force.
- The amount of the cation vacancy in LSM is the important factor.
- The reduction in the $P(O_2)$ gradient under polarized states is the key strategy.

ARTICLE INFO

Article history:
Received 25 April 2013
Received in revised form
26 May 2013
Accepted 28 May 2013
Available online 10 June 2013

Keywords:
Solid oxide fuel cells
Strontium-doped lanthanum manganite
Cathode
Interfacial microstructure
Densification
3D reconstruction

ABSTRACT

Time-dependent events during operation of SOFCs, *i.e.*, performance enhancement and/or deterioration, can be readily observed for the cell composed of strontium-doped lanthanum manganite (LSM) cathode and yttria-stabilized zirconia (YSZ) electrolyte, concomitant with the change in interfacial structure of LSM/YSZ. The influence of LSM composition on the electrochemical properties and microstructure of LSM/YSZ interface during prolonged operation was investigated. Four different LSM cathodes were used and the change in microstructure, especially TPB-length, was evaluated quantitatively by a focused ion beam–scanning electron microscope (FIB–SEM). For LSM cathodes with A-site deficient compositions, the change in TPB-length had a minor contribution to the performance enhancement after 20 h of galvanostatic operation. On the other hand, for 100 h duration an increase in cathode overpotential was confirmed, accompanied with the formation of thin layer of LSM over YSZ electrolyte. A series of phenomena were triggered by the change in oxygen nonstoichiometry of LSM under polarized states. The mechanism for microstructural change was proposed and the long-term stability of LSM/YSZ interface was discussed.

1. Introduction

Strontium-doped lanthanum manganite, $(La,Sr)MnO_{3+\delta}$ (LSM), is one of the promising cathode materials for solid oxide fuel cells (SOFCs), which is a p-type electronic conductor with ABO_3-type perovskite structure. This is primarily due to the chemical and thermal compatibility with yttria-stabilized zirconia (YSZ) electrolytes, high electronic conductivity as well as high electrocatalytic activity for the oxygen reduction reaction. For the cell with LSM cathode/YSZ electrolyte interface, however, the electrochemically active sites are restricted at the triple phase boundary (TPB) of LSM/YSZ/gas because of the low ionic conductivity of LSM. In general, thus, this material is applied as the composite cathode of YSZ–LSM in order to increase the reaction sites and reduce the overpotential.

The cell composed of these materials sometimes exhibits the performance enhancement during the initial cathodic current passage because of the significant reduction in polarization resistance of LSM [1–11]. This activation process is known as the current passage effect, which lasts from several tens of hours to several weeks depending on the composition, operating condition, cell configuration, and fabrication process, etc. In response to this electrochemical behavior, the interfacial microstructure changes continuously with an elapse of time. In the previous study we focused on a series of this phenomenon, and the microstructural change at the $(La_{0.8}Sr_{0.2})_{0.97}MnO_3$/YSZ interface, especially the area-specific TPB-length, upon discharge was quantified by a dual-

* Corresponding author. Tel.: +81 75 383 2523; fax: +81 75 383 2520.
E-mail address: matsui@elech.kuic.kyoto-u.ac.jp (T. Matsui).

0378-7753/$ – see front matter © 2013 Elsevier B.V. All rights reserved.
http://dx.doi.org/10.1016/j.jpowsour.2013.05.162

beam focused ion beam–scanning electron microscope (FIB–SEM) [12]. Although the apparent TPB-length increased by 1.36 times after discharge (0.2 A cm^{-2} for 5 h at 1000 °C in O_2) as compared with that of the as-prepared sample, the rate of increment in active TPB-length was only 7%. Furthermore, almost reversible change in impedance spectra of LSM was observed in the sequential operation of discharge and open-circuit holding, regardless of the irreversible change in interfacial structure. Therefore, it was concluded that an increase in TPB-length had a minor contribution to the current passage effect. The changes in physicochemical properties will be responsible for this process, as suggested by many researchers; *e.g.*, 1) the promotion of oxygen absorption and diffusion over LSM surface [10,13–18], 2) the formation of bulk diffusion path [4,19,20], 3) the removal of passive species such as MnO_x and SrO enriched on LSM surface [9,17,21,22], 4) the expansion of reaction region due to the cation diffusion over electrolyte surface [23,24], and 5) the electrochemical decomposition of insulating phases such as $La_2Zr_2O_7$ formed during the firing process [25–28]. At this stage, however, such a quantitative evaluation was conducted only for $(La_{0.8}Sr_{0.2})_{0.97}MnO_3$ cathode. Since the microstructural change under the polarization must be sensitive to the chemical composition of LSM, a further systematic research is required to make the comprehensive understanding. Moreover, the accumulated operation time is also one of the important factors to be considered because from the long-term view the morphological evolution is unfavorable to assure the durability and reliability of SOFC stack/system.

In this study, we investigated the impact of chemical composition of LSM cathode on the electrochemical properties and microstructure at the LSM/YSZ interface during prolonged operation. Four different LSM cathodes were applied to evaluate the influences of A-site/B-site ratio and La/Sr ratio in the perovskite structure; three A-site deficient LSM with different La/Sr ratio and one A-site rich LSM. The microstructural change upon discharge was quantified by the FIB–SEM analysis and correlated with the electrochemical behavior for each LSM. Furthermore, the mechanism for morphological evolution was proposed and the long-term stability of LSM cathode was discussed.

2. Experimental

Lanthanum strontium manganites, $(La,Sr)MnO_{3+\delta}$, with four-different compositions were prepared as cathodes from corresponding metal acetates (Wako Pure Chemical Industries); $(La_{0.8}Sr_{0.2})_{0.97}MnO_3$, $(La_{0.8}Sr_{0.2})_{1.05}MnO_3$, $(La_{0.6}Sr_{0.4})_{0.97}MnO_3$, and $(La_{0.9}Sr_{0.1})_{0.97}MnO_3$ (hereafter abbreviated as LSM8297, LSM82105, LSM6497, and LSM9197, respectively). The composition expressed for LSM is the nominal one calculated from the ratio of the source regents. Similar nominal expressions are employed for the ratio of A and B components in ABO_3 such as A-site rich and –deficient LSM. Reagents in the required molar ratio were dissolved in water, and then dried at 120 °C. The resulting powder was milled for 24 h and calcined at 900 °C for 10 h, and then mixed with polyethylene glycol (Wako Pure Chemical Industries) to form slurry.

The electrolyte-supported cells were fabricated as follows. A disk of 8 mol% yttria-stabilized zirconia (abbreviated as YSZ, Tosoh, 24 mm in diameter, 500 μm in thickness) was used as the electrolyte. The Ni–YSZ cermet anode with a volume ratio of 50/50 was prepared from NiO (Wako Pure Chemical Industries) and YSZ powder (8 mol% Y_2O_3–ZrO_2, Tosoh). The mixture of NiO and YSZ was heat-treated at 1200 °C for 5 h, and mixed with polyethylene glycol to form slurry. The resultant slurry of NiO–YSZ was screen-printed onto the electrolyte and subsequently fired at 1400 °C for 5 h in air. The other surface of the disk was screen-printed with LSM slurry, and subsequently fired at 1150 °C for 5 h in air. The reference electrode of platinum wire was attached to surround the side edge of the YSZ disk and fixed by a platinum paste (N.E. Chemcat Co., U-3402).

The single cell was sandwiched by alumina tubes with Pyrex glass seal as depicted in our previous report [12]. Prior to electrochemical measurements, the anode was reduced under a hydrogen atmosphere at 1000 °C. The gaseous mixtures of O_2–N_2 and 3% H_2O–97% H_2 were supplied to the cathode and anode, respectively, with a flow rate of 100 mL min^{-1}. Electrochemical measurements were conducted at 1000 °C using the CellTest system (Solartron Analytical, potentiostat/galvanostat 1470E and frequency response analyzer 1455). For the ac impedance measurements, the applied frequency was in the range of 0.1 Hz–500 kHz with voltage amplitude of 10 mV.

The observation of LSM/YSZ interfacial microstructure was carried out using an FIB–SEM setup (NVision 40, Carl Zeiss-SIINT) equipped with an energy dispersive X-ray spectrometer (EDX, Oxford). For the 3D reconstruction of the LSM/YSZ interface, the cell was infiltrated with epoxy resin (Marumoto Struers KK) under vacuum conditions, and then cut and polished. The 2D cross-sectional SEM images (x–y plane) of the LSM/YSZ interface were collected along the z-direction with a spacing of about 50–60 nm by sequential milling-and-observation operation [12,29]. The 3D microstructure of LSM/YSZ interface was virtually reconstructed in a computational field by aligning regularly spaced cross-sectional SEM images.

The LSM cathode was removed by hydrochloric acid treatment in an ultrasonic bath to analyze the top surface of YSZ electrolyte in contact with LSM cathode through SEM observation. This method provides the clean surface of YSZ or secondary phases formed on YSZ electrolyte [25].

3. Results and discussion

The performance changes of four-different LSM cathodes during discharge were monitored. Fig. 1 shows time courses of terminal voltage, cathode overpotential, and ohmic loss between cathode and reference electrode during galvanostatic operation for 20 h. Each measurement was conducted with passing the constant current. The performance enhancement, *i.e.*, current passage effect, was confirmed within *ca.* 1–2 h from the beginning regardless of the cathode composition. After that, except for LSM9197, each cathode exhibited almost constant overpotential as well as ohmic loss up to 20 h. It is noteworthy that the overpotential of LSM9197 increased significantly over duration of 2 h though the current density passed was only 0.2 A cm^{-2}.

In order to assess the influences of La/Sr and A-site/B-site ratios in the perovskite structure of LSM on electrochemical behavior, microstructural changes upon discharge were observed by SEM and compared to each other. Fig. 2 shows the secondary electron (SE) and back-scattered electron (BSE) images of YSZ surface after acid-leaching of LSM8297 cathode, an A-site deficient composition. The cross-sectional images of LSM8297/YSZ interface are also provided. Before discharge the sharply defined convex rings are observed in the SE image, which are considered to correspond to the TPB line [12,25,30,31]. It was reported that these rings were formed by the cation interdiffusion at the LSM/YSZ interface [30–32] and the high concentration of manganese was detected at the convex part of YSZ by the secondary ion mass spectroscopy [30,31]. The corresponding BSE image exhibited mostly uniform contrast; the elements originated from YSZ were only detected by the EDX analysis. Furthermore, LSM8297 particles were tightly adhered to the YSZ surface as can be seen in the cross-sectional image. After current passage for 20 h, however, it was difficult to identify the original convex rings because of an increase in roughness of YSZ both in and out of

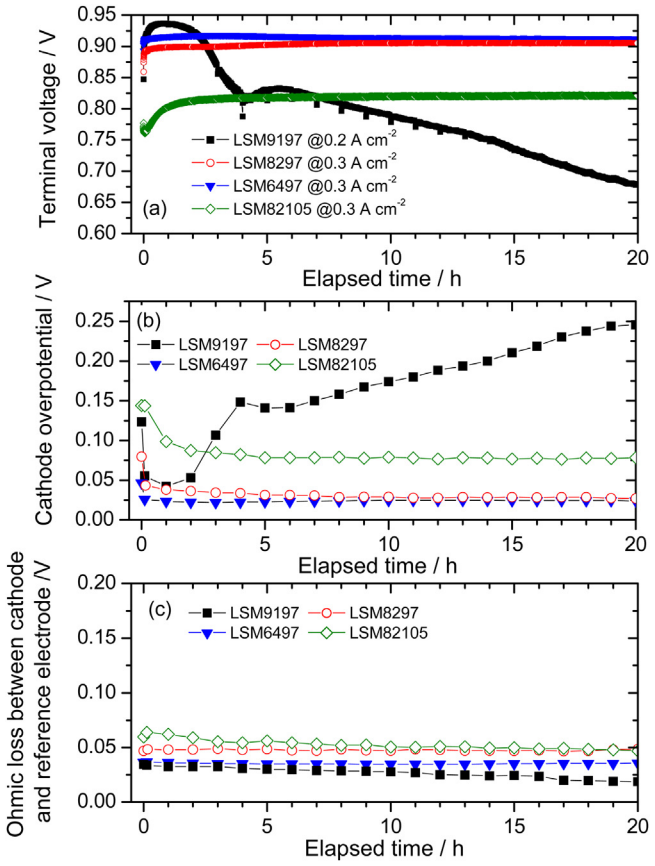

Fig. 1. Time courses of (a) terminal voltage, (b) cathode overpotential, and (c) ohmic loss between cathode and reference electrode for single cells with four different LSM cathodes during discharge at 0.2 A cm^{-2} or 0.3 A cm^{-2} for 20 h. Operating temperature: 1000 °C; Cathode gas: O_2; Anode gas: 3% H_2O–97% H_2.

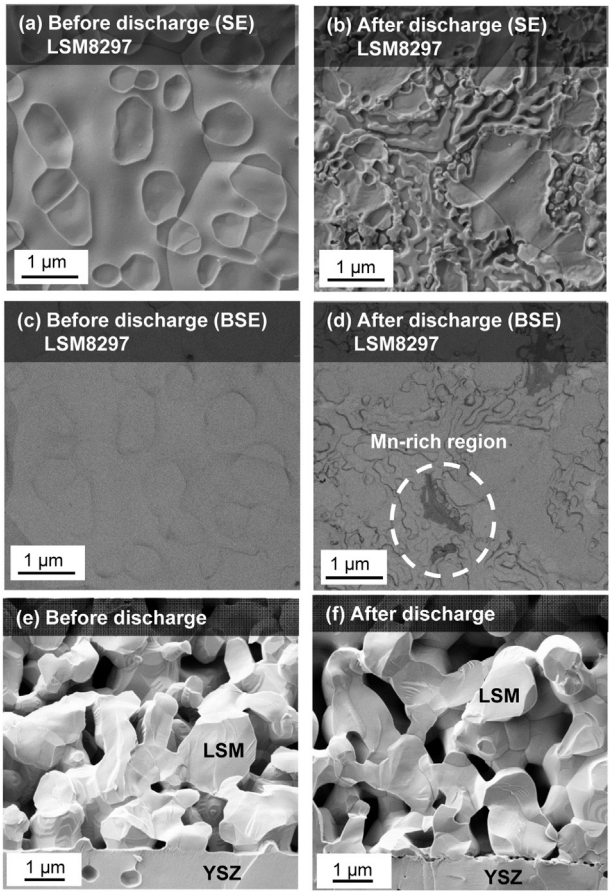

Fig. 2. Microstructural change in LSM8297/YSZ interface before and after discharge at 0.3 A cm^{-2} for 20 h; (a, b) SE and (c, d) BSE images of YSZ surface, and (e, f) cross-sectional SE images of LSM8297/YSZ interface. Operating temperature: 1000 °C; Cathode gas: 100% O_2; Anode gas: 3% H_2O–97% H_2.

contact with LSM8297 particles. Note that in the BSE image, the dark-contrast area has appeared in the vicinity of TPB and the enrichment of manganese was confirmed by the EDX analysis. Therefore, such a Mn-rich region has the potential to affect the performance as reported by several researchers [23,24,33–35]. Furthermore, the solid solution between manganese and YSZ will be formed in these parts considering that manganese oxides are soluble in acid solutions [36]. In response to these morphological changes, small closed pores were formed at the LSM8297/YSZ interface, which were unexposed to the cathode gas. We have reported previously that the microstructural evolution became more complicated with an elapse of current passing time [12]. Upon discharge operation with high current density of 1.2 A cm^{-2}, furthermore, the thin layer of LSM8297 was formed over YSZ electrolyte and became thicker with time (see Fig. 3); this indicated that the high overpotential at LSM cathode promoted the change in interfacial structure, resulting in the reduction in TPB [29]. Therefore, a series of microstructural change at the interface during discharge can be explained by the following mechanism (see Fig. 4). The oxygen potential gradient is formed between TPB and two phase boundary of LSM/YSZ interface when the cathodic current is loaded; the oxygen potential at LSM/YSZ interface is lower than that at TPB under the polarized state because LSM is an electronic conductor in the initial state and oxygen molecules are inaccessible to the interface. Thus, LSM at the two phase boundary tends to be reduced partially, concomitant with the change in oxygen non-stoichiometry. In other words, the metal-rich LSM is formed at the two phase boundary. This means that the formation of concentration gradient of metallic ions leads to the cation diffusion toward the oxygen rich direction.

Analogous microstructural change was observed for the cell with LSM6497, and images are summarized in Fig. 5. The formation of Mn-rich region and closed pores was also confirmed in the vicinity of TPB after discharge. The difference in structural change between LSM6497 and LSM8297 was indiscernible. On the other hand, LSM9197 exhibited the unique structure in its interfacial region as well as on the YSZ surface. Fig. 6 displays the images of YSZ surface and cross-section of LSM9197/YSZ interface. Before discharge there were some undissolved particles on the YSZ surface where was in contact with LSM9197. These particles are ascribable to the $La_2Zr_2O_7$ insulator [37], taking into account the result of EDX analysis (not shown). This solid state reaction originates from the relatively high activity of lanthanum element in LSM9197, but the resultant insulator precipitate had less impact on performance judging from the initial electrochemical performance (Fig. 1). After discharge YSZ surface possessed the complicated structure, and the enrichment of Mn element was unobservable. Moreover, the densification of LSM9197 was observed in the interface region. The blockage of gas diffusion path is the main reason for the drastic increase in overpotential. It is well known that LSM shows the oxygen-excess nonstoichiometry under relatively high oxygen partial pressure [38,39]. Because the amount of excess oxygen reduces with an increase in dopant concentration of Sr in the A-site [38], LSM9197 is regarded as an oxygen-excess composition as compared with LSM8297 and LSM6497. The majority ionic defect in

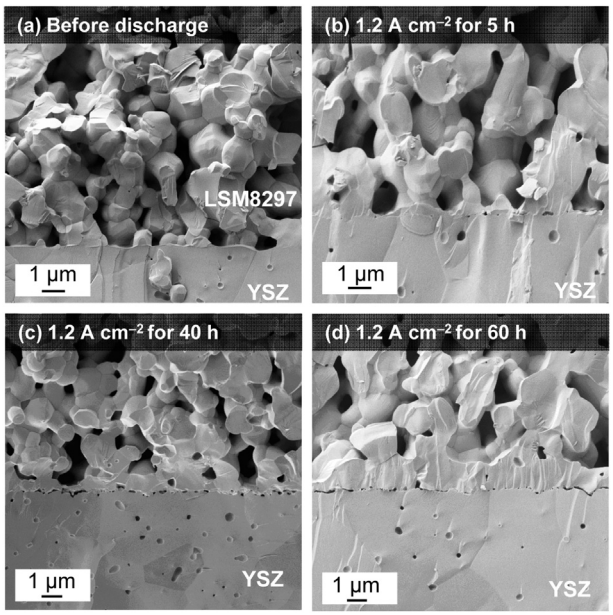

Fig. 3. SE images of cross-section at LSM8297/YSZ interface (a) before and after discharge at 1.2 A cm^{-2} for (b) 5 h, (c) 40 h, and (d) 60 h. Operating temperature: 1000 °C; Cathode gas: O_2. These images are reproduced from our report [29].

LSM is cation vacancies in the oxygen–excess region [39]. Thus, it is considered that a large amount of cation vacancies in LSM9197 leads to the relatively high mobility of cations, based on the proposed mechanism in Fig. 4. The steeper oxygen potential gradient is induced in the vicinity of interface even under the mild discharged condition, 0.2 A cm^{-2}. These results clarified that the La/Sr ratio in the A-site affected remarkably the cation diffusivity, resulting in the difference in microstructural evolution as well as performance change.

Fig. 7 shows YSZ surface images after acid-leaching of LSM82105 cathodes, an A-site rich composition. The surface morphology was quite different from that with LSM8297 both before and after discharge operation. Before discharge YSZ electrolyte possessed a lumpy surface and La element was found present on the entire surface. This suggests the formation of the $La_2Zr_2O_7$ insulator during the initial firing step of cathode. Since the excess amount of lanthanum species is precipitated in the oxide state of La_2O_3 in

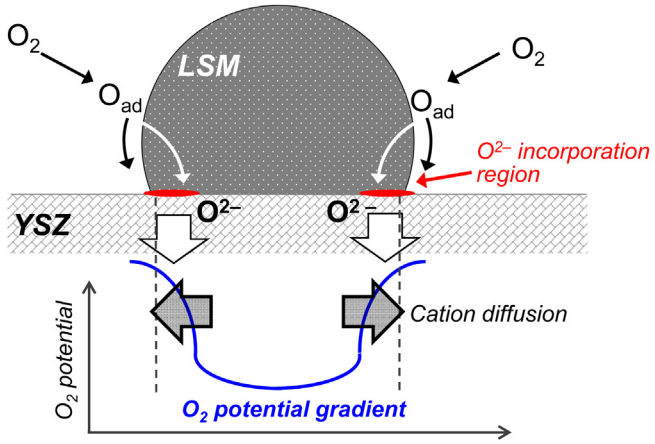

Fig. 4. Schematic diagram for the formation of oxygen potential gradient and cation diffusion in the vicinity of LSM/YSZ interface.

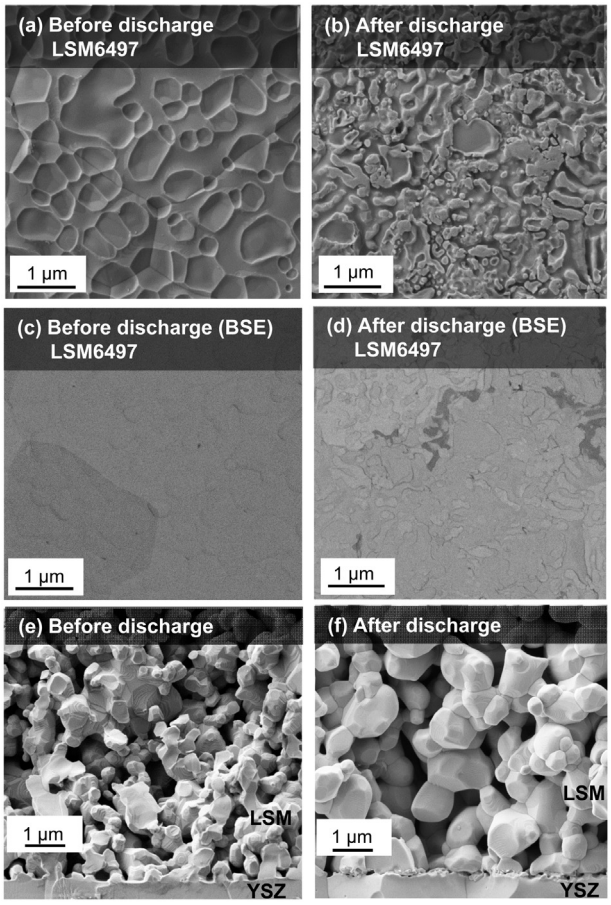

Fig. 5. Microstructural change in LSM6497/YSZ interface before and after discharge at 0.3 A cm^{-2} for 20 h; (a, b) SE and (c, d) BSE images of YSZ surface, and (e, f) cross-sectional SE images of LSM6497/YSZ interface. Operating temperature: 1000 °C; Cathode gas: 100% O_2; Anode gas: 3% H_2O–97% H_2.

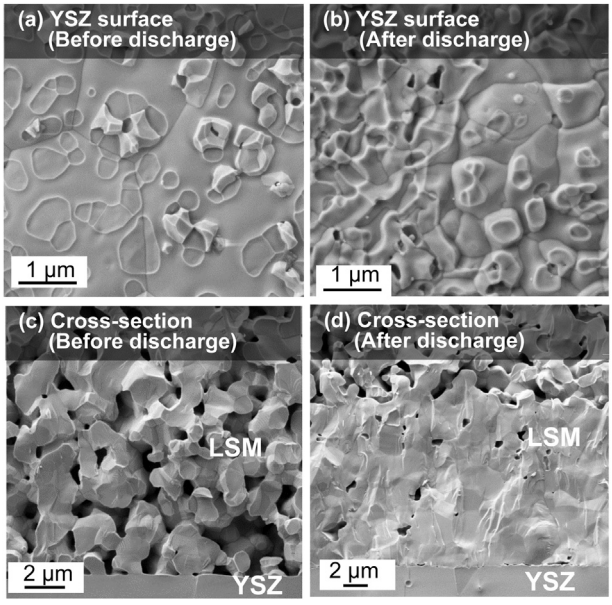

Fig. 6. SE images of (a, b) YSZ surface and (c, d) cross-section at LSM9197/YSZ interface before and after discharge at 0.2 A cm^{-2} for 20 h. LSM9197 was etched by hydrochloric acid for the observation of YSZ surface. Operating temperature: 1000 °C; Cathode gas: 100% O_2; Anode gas: 3% H_2O–97% H_2.

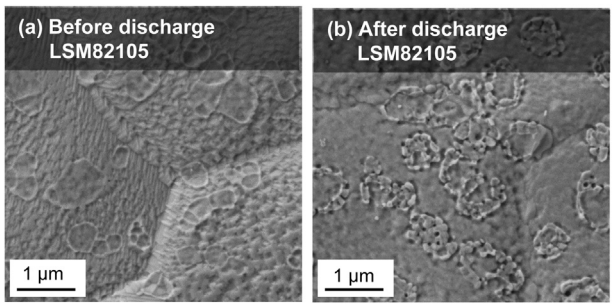

Fig. 7. SE images of YSZ surface (a) before and (b) after discharge at 0.3 A cm^{-2} for 20 h. LSM82105 was used as a cathode and etched by hydrochloric acid. Operating temperature: 1000 °C; Cathode gas: 100% O_2; Anode gas: 3% H_2O–97% H_2.

LSM82105, this oxide reacted with the zirconium component preferentially via the surface diffusion or vaporization–condensation processes [25,33]. After discharge only the surface morphology of YSZ in contact with LSM82105 became rough slightly; the surface out of contact with LSM was scarcely changed. The existence of La element was confirmed by the EDX analysis, but Mn and Sr elements were undetected. Thus, the formation of Mn-rich region was suppressed for LSM82105 cathode, mainly due to the inhibition effect of the insulating $La_2Zr_2O_7$ phase. Moreover, there was no noticeable change in cross-sectional image between LSM82105 and YSZ even after discharge; throughout this study LSM particles were well-adhered to YSZ electrolyte (not shown). However, this composition of LSM82105 is inappropriate for a cathode taking high overpotential into account (Fig. 1). Therefore, A-site/B-site ratio in the chemical formula is also one of the important factors to be considered.

The structural change in each cathode upon discharge was quantified by the FIB–SEM analysis. The sizes of reconstructed samples and the area-specific TPB-length are listed in Table 1. In this study, TPB lines were categorized into two types [12]; the active and inactive TPBs are defined as those exposed and unexposed to the cathode gas, respectively. For instance, the mirror projection of reconstructed LSM6497/YSZ interface is shown in Fig. 8; red and blue lines correspond to the active and inactive TPB lines, respectively. The TPB-length for LSM8297 evaluated in this study was somewhat larger than that of 1.26 μm $μm^{-2}$ in the previous report [12]. This is caused by the individual difference predominantly due to the particle size and viscosity of slurry, considering that the analyzed area was almost the same. Therefore, the cells fabricated from the identical slurry can be comparable quantitatively to each other. The area-specific TPB-length was different depending on LSM compositions before discharge because of the differences in grain size and sinterability. It was obvious that in the initial state, the total TPB-length was almost identical to the active one regardless of compositions, as can be seen in Fig. 8. However, no characteristic correlation was found between the initial performance and area-specific TPB-length. This means that

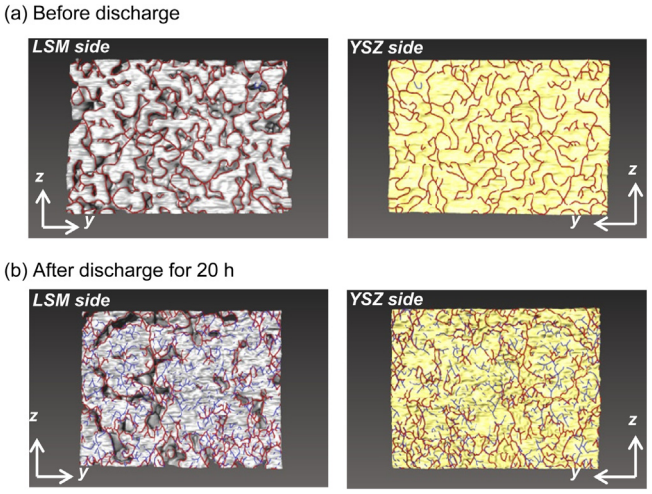

Fig. 8. Mirror projection of LSM6497/YSZ interface, (a) before and (b) after discharge for 20 h. The red and blue lines correspond to the active and inactive TPB lines, respectively. (For interpretation of the references to color in this figure legend, the reader is referred to the web version of this article.)

intrinsic properties, such as the electrocatalytic activity, conductivity of LSM, and/or formation of $La_2Zr_2O_7$ at the interface, are responsible for the initial performance [40]. After discharge, no appreciable increment in active TPB-length was observed for LSM8297 and LSM6497, whereas the total TPB-length increased by *ca.* 9.3% and 41%, respectively. This result reflects the formation of inactive sites especially at the two phase boundary of LSM/YSZ interface (see Fig. 8). Thus, the change in TPB-length had a minor influence on the current passage effect for these cathodes. The performance enhancement upon discharge is mainly dominated by the variation in physicochemical properties of LSM triggered by the change in oxygen nonstoichiometry under polarized states, as described in the introduction part. In the case of LSM82105, the longest TPB-length was almost maintained even after discharge. This phenomenon is related to the reductive decomposition of $La_2Zr_2O_7$ [25] rather than the cation diffusion in LSM under polarization because the performance was enhanced without the noticeable morphological change in LSM82105/YSZ interface. Note that for LSM9197, the number of electrochemically active sites decreased drastically due to the formation of dense layer over YSZ electrolyte. This is the main factor for the performance deterioration, as discussed in the microscopic observation part.

In this study, for LSM8297, the active TPB-length reduced by 16% after passing current for 20 h as listed in Table 1. However, this result is inconsistent with that obtained in our previous report [12]; the slight increase of *ca.* 7% was observed after duration of 5 h at 0.2 A cm^{-2}. This implies that the long-term operation leads to a decrease in active sites and resulting deterioration in performance. Then, the long-term discharge tests were conducted for 100 h. The time course of cathode overpotential during galvanostatic operation and

Table 1
Sizes of the reconstructed samples for the FIB–SEM analysis and area-specific TPB-length.

Sample		LSM8297		LSM82105		LSM6497		LSM9197	
		Before	After	Before	After	Before	After	Before	After
Size of reconstructed sample/μm	*x*	7.03	7.03	7.26	7.03	6.92	7.59	6.48	12.39
	y	10.94	11.28	11.61	10.49	11.61	11.50	10.05	11.83
	z	8.48	8.09	8.96	8.59	8.10	8.96	8.96	8.96
TPB-length/surface area$_{ysz}$/μm $μm^{-2}$	Total[a]	1.61	1.76	2.86	2.57	2.16	3.05	2.24	2.20
	Active[a]	1.61	1.35	2.76	2.52	2.15	2.16	2.23	0.33

[a] Total and active area-specific TPB-lengths were calculated based on the surface area of YSZ electrolyte.

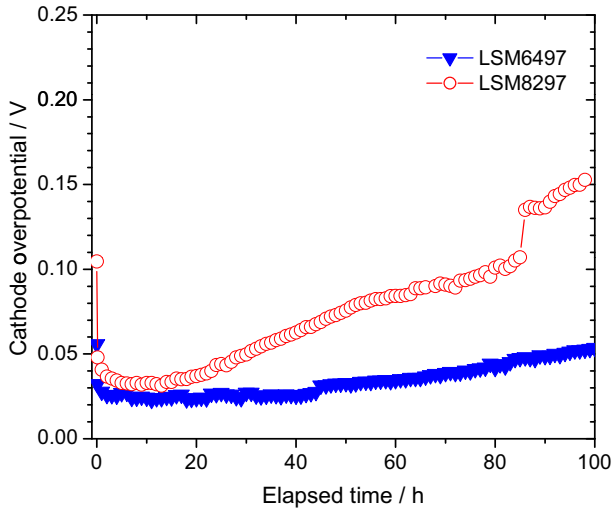

Fig. 9. Time courses of cathode overpotential for single cells with LSM6497 and LSM8297 during discharge at 0.3 A cm^{-2} for 100 h. Operating temperature: 1000 °C; Cathode gas: O_2; Anode gas: 3% H_2O–97% H_2.

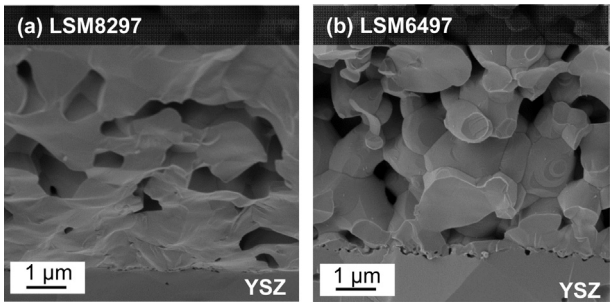

Fig. 10. SE images of cross-section at (a) LSM8297/YSZ and (b) LSM6497/YSZ interfaces after discharge at 0.3 A cm^{-2} for 100 h. Operating temperature: 1000 °C; Cathode gas: O_2; Anode gas: 3% H_2O–97% H_2.

cross-sectional SE images of LSM/YSZ interface after discharge are shown in Figs. 9 and 10, respectively. After the initial performance enhancement, the cathode overpotential was almost stable up to 20 h for both LSM8297 and LSM 6497 cathodes. Afterward, the overpotential was raised with an elapse of time, accompanied with the formation of the LSM thin layer on the YSZ electrolyte. A series of phenomena observed were analogous to that for LSM9197. Note that the deterioration rate and thickness of thin layer formed were different depending on the chemical composition. These are related to the amount of cation vacancy in LSM, which increases with a decrease in doped Sr concentration as discussed above. Therefore, it can be expected that the orders of cation diffusivity and deterioration rate are as follows, LSM9197 > LSM8297 > LSM6497. In fact, this order predicted agreed with the obtained results in this study. These results indicate that the densification of LSM is inevitable and proceeds based on the proposed mechanism during prolonged operation, as long as LSM is applied as a cathode with YSZ electrolyte. Consequently it is revealed that the reduction in the oxygen potential gradient under polarized states is the key design guide to fabricate the stable cathode/electrolyte interface.

4. Conclusions

The influence of LSM composition on the electrochemical properties and microstructure of LSM/YSZ interface during prolonged operation was investigated. The A-site rich LSM was inappropriate for the cathode due to the high overpotential, though the interfacial structure was extremely stable. For three A-site deficient LSM cathodes, the state of interfacial structure upon discharge was significantly affected by the ratio of La/Sr. This is because the amount of cation vacancy in LSM is different depending on the chemical composition. Therefore, the major driving force for the microstructural change was considered to be the oxygen potential gradient between TPB and two phase boundary of LSM/YSZ interface, which was triggered by the change in oxygen non-stoichiometry of LSM under polarized states. Although the current passage effect was observed for these cathodes studied, the change in TPB-length had a minor impact on the performance enhancement. Note that during prolonged operation the formation of thin LSM layer over YSZ electrolyte was observed even under the mild discharged condition, accompanied with an increase in cathode overpotential. This means that the densification of LSM cathode is inevitable. The reduction in the oxygen potential gradient under polarized states is the essential strategy for the development of stable cathode/electrolyte interface.

Acknowledgments

This work was supported by New Energy and Industrial Technology Development Organization (NEDO), Japan (Development of System and Elemental Technology on Solid Oxide Fuel Cell Project).

References

[1] S.B. Adler, Chem. Rev. 104 (2004) 4791.
[2] S.P. Jiang, J. Mater. Sci. 43 (2008) 6799.
[3] H. Tsukuda, A. Yamashita, K. Hasezaki, J. Ceram. Soc. Jpn. 105 (1997) 862.
[4] X.J. Chen, K.A. Khor, S.H. Chan, J. Power Sources 123 (2003) 17.
[5] A.A. Vance, S. McIntosh, J. Electrochem. Soc. 155 (2008) B1.
[6] S. Koch, M. Mogensenm, P.V. Hendriksen, N. Dekker, B. Rietveld, Fuel Cells 6 (2006) 117.
[7] S.P. Jiang, J.G. Love, Solid State Ionics 158 (2003) 45.
[8] K. Murakami, T. Matsui, R. Kikuchi, H. Muroyama, K. Eguchi, J. Electrochem. Soc. 157 (2010) B880.
[9] M.A. Haider, S. McIntosh, J. Electrochem. Soc. 156 (2009) B1369.
[10] F.H. van Heuveln, H.J.M. Bouwmeester, J. Electrochem. Soc. 144 (1997) 134.
[11] W. Wang, S.P. Jiang, J. Solid State Electrochem. 8 (2004) 914.
[12] T. Matsui, Y. Mikami, H. Muroyama, K. Eguchi, J. Electrochem. Soc. 157 (2010) B1790.
[13] J.D. Kim, G.D. Kim, J.W. Moon, Y.I. Park, W.H. Lee, K. Kobayashi, M. Nagai, C.E. Kim, Solid State Ionics 143 (2001) 379.
[14] K. Yasumoto, N. Mori, J. Mizusaki, H. Tagawa, M. Dokiya, J. Electrochem. Soc. 148 (2001) A105.
[15] K. Yasumoto, M. Shiono, H. Tagawa, M. Dokiya, K. Hirano, J. Mizusaki, J. Electrochem. Soc. 149 (2002) A531.
[16] X.J. Chen, K.A. Khor, S.H. Chan, Solid State Ionics 167 (2004) 379.
[17] S.P. Jiang, J. Solid State Electrochem. 11 (2007) 93.
[18] X.J. Chen, S.H. Chan, K.A. Khor, Electrochem. Solid-State Lett. 7 (2004) A144.
[19] T. Horita, K. Yamaji, N. Sakai, H. Yokokawa, T. Kawada, T. Kato, Solid State Ionics 127 (2000) 55.
[20] T. Horita, K. Yamaji, M. Ishikawa, N. Sakai, H. Yokokawa, T. Kawada, T. Kato, J. Electrochem. Soc. 145 (1998) 3196.
[21] S.P. Jiang, J.G. Love, Solid State Ionics 138 (2001) 183.
[22] W. Wang, S.P. Jiang, Solid State Ionics 177 (2006) 1361.
[23] M. Backhaus-Ricoult, K. Adib, T.St. Clair, B. Luerssen, L. Gregoratti, A. Barinov, Solid State Ionics 179 (2008) 891.
[24] M. Backhaus-Ricoult, Solid State Sci. 10 (2008) 670.
[25] A. Mitterdorfer, L.J. Gauckler, Solid State Ionics 111 (1998) 185.
[26] S.P. Jiang, J.G. Love, J.P. Zhang, M. Hoang, Y. Ramprakash, A.E. Hughes, S.P.S. Badwal, Solid State Ionics 121 (1998) 1.
[27] E. Ivers-Tiffée, A. Weber, K. Schmid, V. Krebs, Solid State Ionics 174 (2004) 223.
[28] A. Weber, R. Männer, R. Waser, E. Ivers-Tiffée, Denki Kagaku 64 (1996) 582.
[29] J. Yang, H. Muroyama, T. Matsui, K. Eguchi, J. Power Sources 204 (2012) 25.
[30] T. Horita, T. Tsunoda, K. Yamaji, N. Sakai, T. Kato, H. Yokokawa, Solid State Ionics 152–153 (2002) 439.
[31] S.P. Jiang, W. Wang, Electrochem. Solid-State Lett. 8 (2005) A115.
[32] M. Kuznecov, P. Otschik, P. Obenaus, K. Eichler, W. Schaffrath, Solid State Ionics 157 (2003) 371.
[33] F. Zheng, L.R. Pederson, J. Electrochem. Soc. 146 (1999) 2810.
[34] C. Chung, T. Yang, W. Cheng, J. Wei, J. Am. Ceram. Soc. 87 (2004) 1110.
[35] M. Backhaus-Ricoult, Solid State Ionics 177 (2006) 2195.
[36] J. Mizusaki, Solid State Ionics 86–88 (1996) 1335.

[37] J.A.M. van Roosmalen, E.H.P. Cordfunke, Solid State Ionics 52 (1992) 303.
[38] J. Mizusaki, N. Mori, H. Takai, Y. Yonemura, H. Minamiue, H. Tagawa, M. Dokiya, H. Inaba, K. Naraya, T. Sasamoto, T. Hashimoto, Solid State Ionics 129 (2000) 163.
[39] S. Miyoshi, J.O. Hong, K. Yashiro, A. Kaimai, Y. Nigara, K. Kawamura, T. Kawada, J. Mizusaki, Solid State Ionics 154–155 (2002) 257.
[40] A. Chen, J.R. Smith, K.L. Duncan, R.T. DeHoff, K.S. Jones, E.D. Wachsman, J. Electrochem. Soc. 157 (2010) B1624.